Porous Co_3O_4 hollow nanododecahedra for Nonenzymatic glucose biosensor and biofuel cell

Erhuan Zhang, Yu Xie, Suqin Ci, Jingchun Jia, Zhenhai Wen

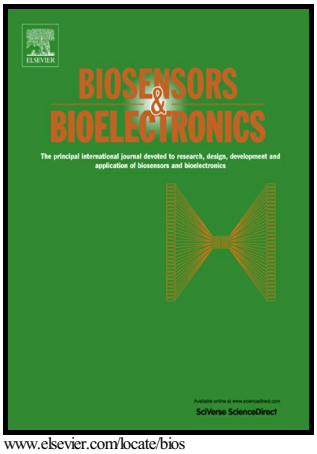

www.elsevier.com/locate/bios

PII: S0956-5663(16)30133-6
DOI: http://dx.doi.org/10.1016/j.bios.2016.02.027
Reference: BIOS8459

To appear in: *Biosensors and Bioelectronic*

Received date: 27 November 2015
Revised date: 2 February 2016
Accepted date: 9 February 2016

Cite this article as: Erhuan Zhang, Yu Xie, Suqin Ci, Jingchun Jia and Zhenha Wen, Porous Co_3O_4 hollow nanododecahedra for Nonenzymatic glucos biosensor and biofuel cell, *Biosensors and Bioelectronic* http://dx.doi.org/10.1016/j.bios.2016.02.027

Porous Co_3O_4 Hollow Nanododecahedra for Nonenzymatic Glucose Biosensor and Biofuel Cell

Erhuan Zhang,[1,2] Yu Xie,[1*] Suqin Ci,[1] Jingchun Jia,[2,3] Zhenhai Wen[1,2,3*]

1 Key Laboratory of Jiangxi Province for Persistent Pollutants Control and Resources Recycle, Nanchang Hangkong University, Nanchang 330063, PR China

2 Key Laboratory of Design and Assembly of Functional Nanostructures, Fujian Institute of Research on the Structure of Matter, Chinese Academy of Sciences, Fuzhou, Fujian 350002, P. R. China

3 Fujian Provincial Key Laboratory of Nanomaterials, Fujian Institute of Research on the Structure of Matter, Chinese Academy of Sciences, Fuzhou, Fujian 350002, P. R. China

E-mail: wenzhenhai@yahoo.com or wen@fjirsm.ac.cn

Abstract: Cobalt oxide hollow nanododecahedra (Co_3O_4-HND) is synthesized by a facile thermal transformation of cobalt-based metal-organic framework (Co-MOF, ZIF-67) template. The morphology and properties of the Co_3O_4-HND are characterized by a set of techniques, including transmission electron microscope (TEM), powder X-ray diffraction (XRD), scanning electron microscope (SEM) and Brunner-Emmet-Teller (BET). When tested as a non-enzymatic electrocatalyst for glucose oxidation reaction, the Co_3O_4-HND exhibits a high activity and shows an outstanding performance for determining glucose with a wide window of 2.0 μM-6.06 mM, a high sensitivity of 708.4 μA $mM^{-1}cm^{-2}$, a low detection limit of 0.58 μM (S/N= 3), and fast response time(< 2 s). Based on the nonenzymatic oxidation of glucose, Co_3O_4-HND could be served as an attractive non-enzyme and noble-metal-free

electrocatalyst in glucose fuel cell (GFC) due to its excellent electrochemical properties, low cost and facile preparation.

Key words: Hollow Co_3O_4 nanododecahedra, Nonenzyme, Glucose biosensor, Glucose fuel cell

1. Introduction

In recent years, there is no doubt that hollow nanostructured materials are widely performed for a wide range of application in many important fields, such as catalysis(Kim et al. 2002), drug delivery,(Li et al. 2003) and energy storage(Hu et al. 2015; Lou et al. 2006), owing to their unique properties, such as lower mass density, higher porosity, higher surface area, and so forth. Typically, the hollow structured materials can be prepared by either hard templates or soft template methods. Unfortunately, these approaches require complex steps to remove templates or etch using some corrosive solvent, which would induce some impure materials in the final product and thus limit the extensive applications of hollow nanomaterials. Despite great progress have been made recently, it still remains a challenge for developing a simple and feasible protocol for the synthesis of hollow nanostructures with well-defined geometries.

Development of glucose sensors is of paramount importance in a variety of fields, especially for applications of blood glucose testing, environmental monitoring, pharmaceutical analysis and energy conversion. Non-enzymatic detection of glucose has become a hotspot in recent years because it is a potential alternative technique to solve the disadvantages of enzymatic biosensors.(Si et al. 2013; Wang et al. 2013) Additionally, Biofuel cells (BFCs) are promising next-generation energy devices which are able to use enzymes or microorganisms as catalysts to harvest electrical energy from chemical energy of a fuel in gentle and environmental-friendly conditions(Cooney et al. 2008). There exists significant overlap in technical requirements between sensors and Biofuel cell (BFC), including chemical and mechanical stability, selectivity, and cost of materials(Calabrese Barton et al. 2004).

In principle, most enzymatic BFCs use glucose as the fuel due to its vast abundance, ready availability, and environmental-friendly chemistry. Typically, enzymes were used as the catalysts of glucose biosensors and BFC, but they are susceptible to the operating environment and suffer from fragile stability(Yuhashi et al. 2005). To overcome the drawbacks of enzyme electrodes, various nonenzymatic glucose and fuel cells introducing metal-based nanomaterials as catalysts have been fabricated. Non-enzyme electrocatalysts based on noble metals (e.g., Pt, Au, or their alloys) could be option for glucose fuel cell (GFC) due to their considerable activity for glucose oxidation reaction (GOR)(Basu and Basu 2011). However, their applications are limited by surface poisoning of adsorbed intermediates from the oxidation of glucose, apart from their scarcity and high cost.

Transition-metal oxides, such as NiO,(Ci et al. 2014; Mu et al. 2011) Co_3O_4,(Wang et al. 2012) CuO,(Song et al. 2013) etc., have recently received great extended attention in glucose electrochemical oxidation due to their pronounced properties, such as low cost and good biocompatibility compared with noble metal-based materials.(Li et al. 2015; Yang et al. 2015) Among the materials mentioned above, Co_3O_4 nanocomposite have drawn more attention as a result of their enhanced electrocatalytic behavior and good response stability, and thus have been extensively used in enzyme-free glucose sensors and other electrochemical applications.(Madhu et al. 2015) Moreover, Co/NG and Co_3O_4 hybridized 3D graphene electrodes are served as the anode for glucose oxidation to harvest energy from green and sustainable glucose fuel (Chen et al. 2013; Ci et al. 2015b). Nevertheless, there has been rarely studied in producing hollow transition oxide from uniform template with regular morphology to serve as a glucose sensor, or designing glucose fuel cells based on the nonenzymatic oxidation of glucose, despite the fact that the hollow structure and

corresponding properties, such as well-defined interior voids, high specific surface area, low density, and structural stability, may bring about a sensor with various advantages including high sensitivity, good stability, and low detection limit.

To date, metal-organic frameworks (MOFs), a novel of porous materials synthesized by assembling metal ions with rigid organic molecules, have stimulated a great deal of interest in gas storage and separation, catalysis, and biomedicine as a result of their tunable porosity, and a tailored chemical property, as well as versatile applications.(Horcajada et al. 2010; Lee et al. 2009; Li et al. 2011a; Sculley et al. 2011) In addition, MOFs have been demonstrated to be the sacrificial templates for fabricating porous metal oxides or carbon nanostructures via thermal decomposition under controlled atmosphere. Interestingly, the porosity and long-range ordering of MOFs can impart their MOF-derived hollow structures some unique features. On one hand, the MOF-derived hollow structures inherits the precursor's morphology; on the other hand, the pores in MOF-derived hollow materials, which are distinct from "dead pores", contact each other since they were generated from gas molecules release. Recently, it was reported that the porous Co_3O_4 nanododecahedra can be successfully prepared through calcination of Co-based zeolitic imidazolate framework (ZIF-67) under an oxygen atmosphere, As a result, such nanostructured Co_3O_4 possesses a high specific surface area, electrochemical active area and good biocompatibility.(Hou et al. 2015; Hu et al. 2015; Huang et al. 2015; Lü et al. 2014; Shao et al. 2014; Wang et al. 2015; Wu et al. 2014; Zhang et al. 2014)

Herein, we present an effective approach for preparing hollow Co_3O_4-HND nanostructures by one-step pyrolysis of the rhombic dodecahedral ZIF-67 precursor. The obtained hollow Co_3O_4 with polyhedral structures has been evidenced as a high-

active catalyst which can directly detect glucose without need of any enzymes. Notably, Co_3O_4-HND exhibit outstanding electrocatalytic activity for glucose oxidation reaction (GOR), empowering us to build a rational precious-metal-free glucose fuel cell (GFC).

2. Materials and methods

2.1. Materials

Ascorbic acid (AA), uric acid (UA), dopamine (DA), β-D-Glucose, fructose, lactose, sucrose, mannose, maltose were purchased from Bomei Company. Nafion, Cobalt nitrate hexahydrate ($Co(NO_3)_2 \cdot 6H_2O$, 99%), 2-methylimidazole (mIM, 99%), bulk Co_3O_4, and KOH were purchased from Aladdin. N-methylpyrrolidinone (NMP), polyvinylidene fluoride (PVDF) binder, Super-P carbon black, carbon cloth and Pt/C (20%) were bought from sigma-aldrich. All aqueous solutions were freshly acquired with high purity water (≥18 MΩ cm) generated from a Gen Pure UV-TOC/UF ultra-pure water system (TKA, Niederelbert, Germany).

2.2. Synthesis of samples

The present protocol to synthesize porous Co_3O_4-HND involved a two-step route, including optimization of ZIF-67 and following calcination treatment at 300 ℃. In the first step, ZIF-67 crystals were synthesized by a room-temperature precipitation. Typically, $Co(NO_3)_2 \cdot 6H_2O$ (0.45 g) was dissolved in 3 mL deionized water, then 2-methylimidazole (5.5 g) in 20 mL of water was added into above solution under vigorously stirred for 6 h at room temperature (RT). The resulting purple precipitates

were collected by centrifugation and washed with ethanol several times and finally vacuum-dried at 80 ºC for 24 h. In the second step, a combustion boat loaded the ZIF-67 powders was directly placed in a tube furnace. The temperature inside the furnace was gradually increased from room temperature to the target temperature with a heating rate of 5 ºC·min^{-1}. After the powder was annealed for 3 h at 300 ºC under air, the purple precursor was finally converted into the black product.

2.3. Apparatus measurements

The morphology and structure of powder were captured with a transmission electron microscope (TEM, JEM-2010) and a scanning electron microscope (SEM, NOVA NANOSEM450). Power X-ray diffraction (XRD) was conducted on a Bruker D8 advance diffractometer at 40 mA and 40 KV, using Cu Kα (λ= 1.5418Å) radiation. The thermogravimetry analysis (TGA) of sample was recorded with a Netzsch STA 449 thermogravimetric analyzer at a heating rate of 10 ºC/ min in air. Specific surface area, pore volume and pore size distribution of the products was examined by the Brunauer-Emmett-Teller (BET) method using nitrogen adsorption and desorption isotherms on a Micromeritics Instrument Corporation sorption analyzer (Micromeritics TriStar II 3020). FT-IR spectra was measured by a Nicolet Magna-IR 560 spectrophotometer (Bruker, Germany).

2.4. Electrochemical measurements

The modified electrode was prepared as follows: the glass carbon electrode (GCE) was polished with alumina slurry, and then ultrasonically cleaned alternately in ethanol-and double-distilled water. Co_3O_4-HND (2.5 mg), 0.05 mL Nafion solution and 0.03mL ethanol were dispersed in 420mL distilled water to form a homogeneous ink. Then 6 μL of the mixture was dropped onto the cleaned GCE, and allowed to dry

at room temperature. All electrochemical measurements were carried out on a CHI 604E electrochemical analyzer (Shanghai, China) using the conventional three-electrode configuration with a 0.1 M KOH solution as the electrolyte, in which the glassy carbon modified with Co_3O_4-HND was served as working electrode, a platinum wire as counter electrode and Ag/AgCl electrode as reference electrode, respectively. All of the electrochemical performance experiments were performed at room temperature (25ºC) with a magnetic stirrer. Meanwhile, all solutions were deoxygenated with highly pure argon (99.99%) for at least 15 min before tests. In the test, all potentials were referred to Ag/AgCl reference electrode, the geometric surface area of the modified electrode (0.07 cm^2) was calculated the current density. The electrochemical glucose detection performance was investigated by chronoamperometry and cyclic voltammetry (CV) in the region from 0 V to 0.7V.

The Fuel cell (FC), made in house with acrylic glass, was separated by a proton exchange membrane as the anodic and cathodic compartments. The cell voltage was measured by a digital multimeter (Keithley Instruments, Inc. Cleveland, OHIO, USA). Co_3O_4-HND electrode was successfully designed with the following method: 15 mg (Co_3O_4-HND) was added to 100 mg NMP solvent containing 3 mg Super-P carbon black and 1 mg PVDF. The suspension was mixed together and homogenized. Here, 0.1 M KOH/0.1 M Glucose solution served as electrolyte. The mixed solution was injected in the cathodic chamber at constant flow (5 mL/min) using maximum volume 50 mL injector. The 0.1 M KOH solution was added into the cathodic compartment which was exposed to air under “breathing” environment. The active area of carbon cloth was 1×3 cm^2. The FC was linked with external resistance of 200 Ω, and the corresponding output voltage value with time was recorded at 25 °C by a precision digital multimeter.

3. Result and disscussion

3.1. Characterization

The crystallographic structure and phase purity were examined by X-ray diffraction (XRD) measurement. Figure 1a shows the XRD pattern of the ZIF-67, in which all peaks are in agreement with previous reports.(Wu et al. 2014) Figure 1b presents the XRD pattern of the product, i.e. Co_3O_4-HND, derived from ZIF-67, the diffraction peaks at 2θ values of 19.0°, 31.3°, 36.8°, 38.5°, 44.8°, 56.6°, 59.3°, 65.2° can be well indexed to the (111), (220), (331), (222), (400), (422), (511), (440) crystal planes of the pure spinel-type Co_3O_4 (JCPDS Card No.43-1003). The XRD analysis demonstrated that the ZIF-67 was completely converted into pure Co_3O_4. Remarkably, the XRD peaks are broaden in width and weaken in intensity, indicating that the Co_3O_4-HND crystallites are actually built by lots of Co_3O_4 nanoparticles. No diffraction peaks from residues or impurities are observed, corresponding to the phase of pure Co_3O_4. For comparison, the XRD pattern of bulk Co_3O_4 (red line) was obtained in Figure 1b.

To achieve a better understanding on the evolution from ZIF-67 to Co_3O_4-HND, a thermal gravity analysis was conducted on ZIF-67 to investigate the thermal properties. Figure 1c displays the weight change curve of ZIF-67 determined by thermogravimetric analysis (TGA). The weight loss occurs over two different temperature ranges. The first slightly weight loss below 250 ºC and can be attributed to the evaporation of physically adsorped water; the second major weight loss process in the range of 250-450 ºC corresponded with the decomposition of the ZIF-67 framwork that released a large amout of gas including of H_2O, CO_2, and NO_x. No

significant weight loss is observed at temperatures above 500 ºC, suggesting that ZIF-67 was decomposed completely and transformed into stable Co_3O_4 hollow structure.

Since the ZIF-67 possesses a high porosity, a large pore volume, a low mass-to-volume ratio of metal ions, and a large structural strain, most of which will be maintained in the transformation process from ZIF-67 to Co_3O_4.(Lü et al. 2014) To evaluate the specific surface area and the porosity of the porous hollow Co_3O_4 dodecahedral structure, N_2 adsorption-desorption isotherm and BJH pore size distribution analysis are performed (Figure 1d). The specific surface area of Co_3O_4-HND is calculated to be 62.5 m^2/g by the BET analysis. In addition, Co_3O_4-HND exhibits an isotherm of type IV, indicating the presence of mesopores.(Li et al. 2011b) The plot of pore size distribution determined by the BJH analysis shows the distribution of pores is in the mesoporous range of 2.8-32.5 nm with maxima at around 9.9 nm (inset of Figure 1d).

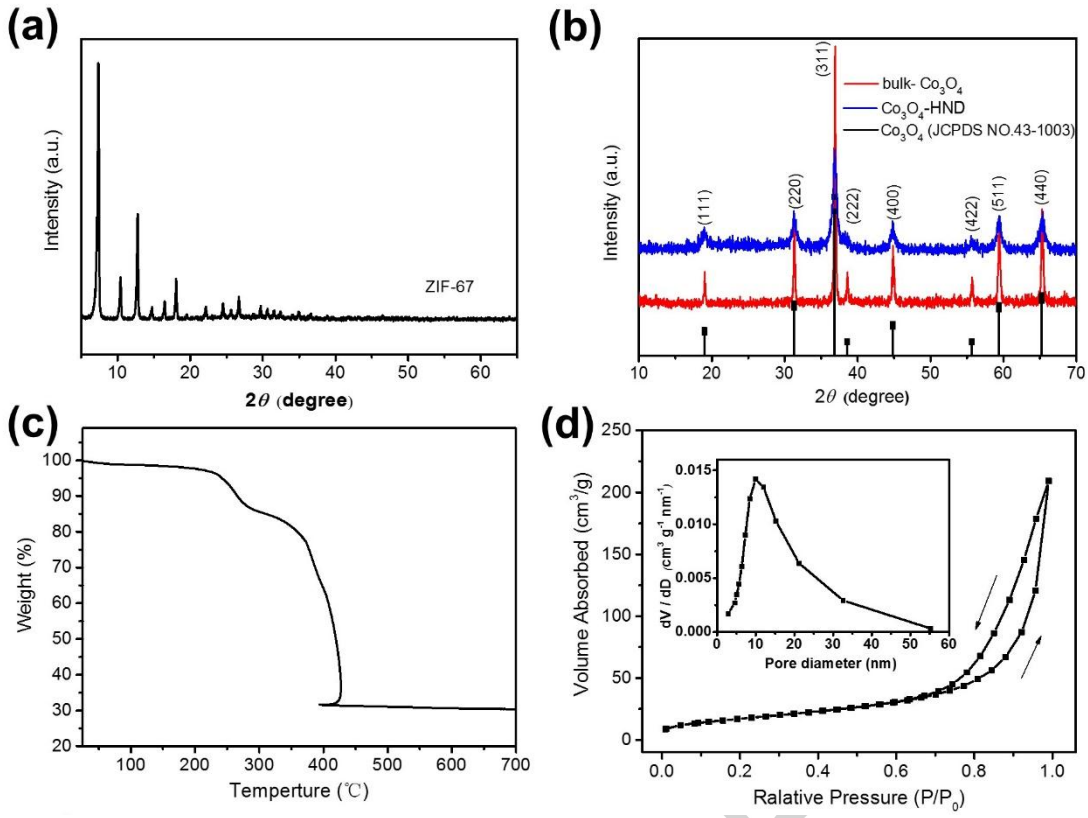

Figure 1. (a) XRD pattern of the ZIF-67; (b) XRD patterns of porous Co_3O_4-HND obtained by calcination in air and bulk Co_3O_4; (c) TGA curve of the as-prepared ZIF-67; (d) Nitrogen adsorption-desorption isotherm of porous Co_3O_4. Inset shows pore size distribution calculated from desorption branch of the isotherm with BJH method.

The morphology of ZIF-67 and Co_3O_4 were examined by SEM, as shown in Figure 2, we can observe that the ZIF-67 particles have a well-defined dodecahedron with a size range of 200-300 nm (Figure 2a). As depicted in Figure 2b and 2c, FESEM images of Co_3O_4-HND with different magnifications demonstrate that Co_3O_4-HND inherites very well the dimension and shape of ZIF-67 precursor. Additionally, it can be clearly observed that the surface of concave dodecahedra was very rough, suggesting the presence of abundant pores during calcination process. For

comparison, the bulk Co_3O_4 was also characterized by SEM, as shown in Figure 2d, illustrating bulk Co_3O_4 with disorder structure.

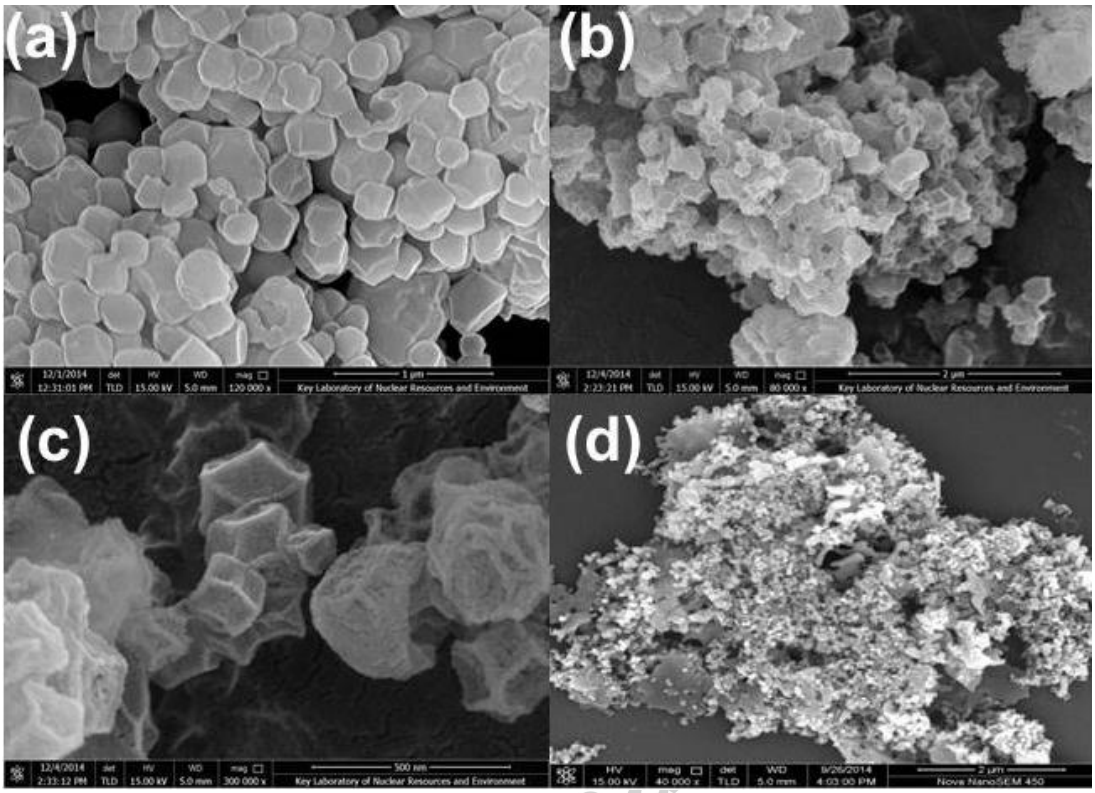

Figure 2. (a) FESEM image of Co-MOF precursor (b) Low- and (c) high-magnified FESEM images of Co_3O_4-HND and (d) FESEM image of bulk Co_3O_4.

Figure 3a reveals a typical transmission electron microscopy (TEM) image of the Co_3O_4-HND, the projection profiles of most particles remain well consistent with the concave dodecahedra precursor. The brighter contrast in center region of squares confirms that each polyhedron consisting of a hollow structure is built by a large amount nanoparticles with formation of lots of pores (Figure 3b). From the high-resolution TEM (HRTEM) image of Co_3O_4 shown in Figure 3c, the center region of a Co_3O_4 dodecahedra whose nanoparticles have a size range of 2-6 nm with observable lattice spacings of 0.46nm and 0.28 nm, respectively, which is assignable to the (111)

and (220) lattice plane of Co_3O_4. Close observation on TEM image demonstrates the Co_3O_4 nanocrystallines are attached with each other. The corresponding selective-area electron diffraction (SAED) pattern (Figure 3d) of the Co_3O_4-HND presents several concentric rings, which can be attributed to diffraction planes of the Co_3O_4 and is well consistent with the XRD results(Figure 1b), further indicating that Co_3O_4 have a good crystalline structure.

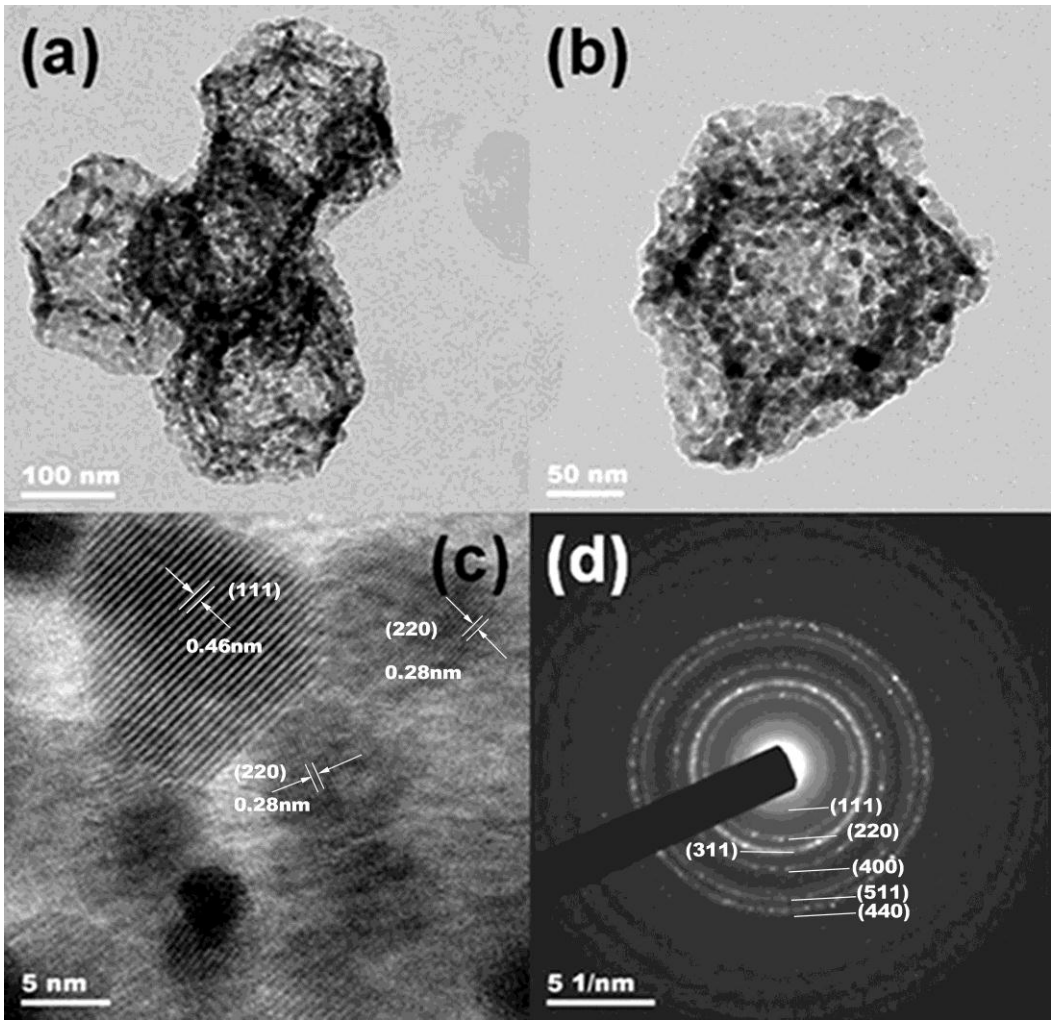

Figure 3. (a,b) TEM images of Co_3O_4 -HND; (c) HRTEM images of Co_3O_4 hollow dodecahedra; (d) SAED pattern of Co_3O_4 -HND.

Based on the aforementioned analysis results, it is evidenced that ZIF-67 is subjected to a heterogeneous contraction process induced by a non-equilibrium heat-treatment approaches during the formation of Co_3O_4-HND.(Guan et al. 2010) An initial Co_3O_4 shell is formed on the surface of ZIF-67 at the beginning of thermal oxidation of these particles. Although this thin shell together with external precursor coating play the role of an interface to get detached the inner ZIF-67 from the outer atmospheric oxygen, the outward diffusion of ZIF-67 occurred as a result of a large number of vacancies in the interface. The precursor inward gradually transforms into Co_3O_4 core and separated from the performed outer shell with the increasing temperature, which are attributed to synergistic effect of the adhesion and contraction forces. The inward diffusion rate of atmospheric oxygen is much smaller than ZIF-67, finally leading to a hollow cavity. As expected, the porous dodecahedra consisted of nanoparticle was successfully assembled.

3.2. Electrochemical behavior of the Co_3O_4 -HND

Initially, the electrochemical properties of the Co_3O_4-HND and bulk Co_3O_4 were investigated in 0.1 M KOH electrolyte. The CV tests were performed in the range from 0 V to 0.7 V vs. Ag/AgCl. Figure 4a and Figure S1 show the CV curves of the Co_3O_4-HND electrode and bulk Co_3O_4 electrode in the absence (red line) and presence (black line) of glucose. Both Co_3O_4 -HND and bulk Co_3O_4 display two pairs of redox peaks with anodic peaks at around 0.55 V and 0.32 V and cathodic peaks at around 0.48 V and 0.25 V, respectively. The pair of redox peaks I/II labeled in dotted line are poorly defined and can be attributed to the conversion between Co_3O_4 and CoOOH, while the other pair of peaks III/IV can be assigned to the reversible transition between CoOOH and CoO_2.(Ding et al. 2010) Apparently, the Co_3O_4-HND

shows much higher electrochemical response upon addition of glucose than the bulk Co_3O_4, as is evidenced by a higher peak current density at the Co_3O_4 -HND electrode. Notably, with addition of glucose, peak III was even stronger than that peak I, suggesting the electro-oxidation of glucose is mainly catalyzed by $CoOOH/CoO_2$ rather than $Co_3O_4/CoOOH$. These two reversible reactions can be expressed as the following equation (1) and (2)：

$$Co_3O_4 + OH^- + H_2O \leftrightarrow 3CoOOH + e^- \quad (1)$$

$$CoOOH + OH^- \leftrightarrow CoO_2 + H_2O + e^- \quad (2)$$

The anodic current density increase accordingly with the enhancement of glucose concentration accompanying with the decrease of cathodic current density (Figure S1). The mechanism of electrochemical oxidation of glucose catalyzed by Co-based compounds could be presumably proposed as the following (Ding et al. 2010; Han et al. 2015):

$$2CoO_2 + C_6H_{12}O_6 \leftrightarrow 2CoOOH + C_6H_{10}O_6 \quad (3)$$

In this way, the forward reaction between CoO_2 and CoOOH in equation (3) would be greatly favored with increasing glucose concentration and thus resulting in an enhanced for peak III, suggesting the electro-oxidation reaction of glucose occur with the consumption of CoO_2, which in turn results in the slight decrease of cathodic peak current, i.e. the reverse reaction of equation (2), with the increase of glucose.

The relationship between the current density and the scan rate was revealed in Figure S2a. From CVs of the Co_3O_4-HND at the scan rate ranging from 5 to 120mV s^{-1}, it is noted that the anodic peak presents a slight positive shift while the cathodic

peak shifts negatively with the increase in scan rate, indicating a quasi-reversible electron transfer reaction for the above redox reaction. As depicted in Figure S2b, the peak current densities for both the oxidation and the reduction currents are proportional to the square root of the scan rate, implying that the electrochemical reaction on the electrode surface is a diffusion-controlled process.(Zhang et al. 2015)

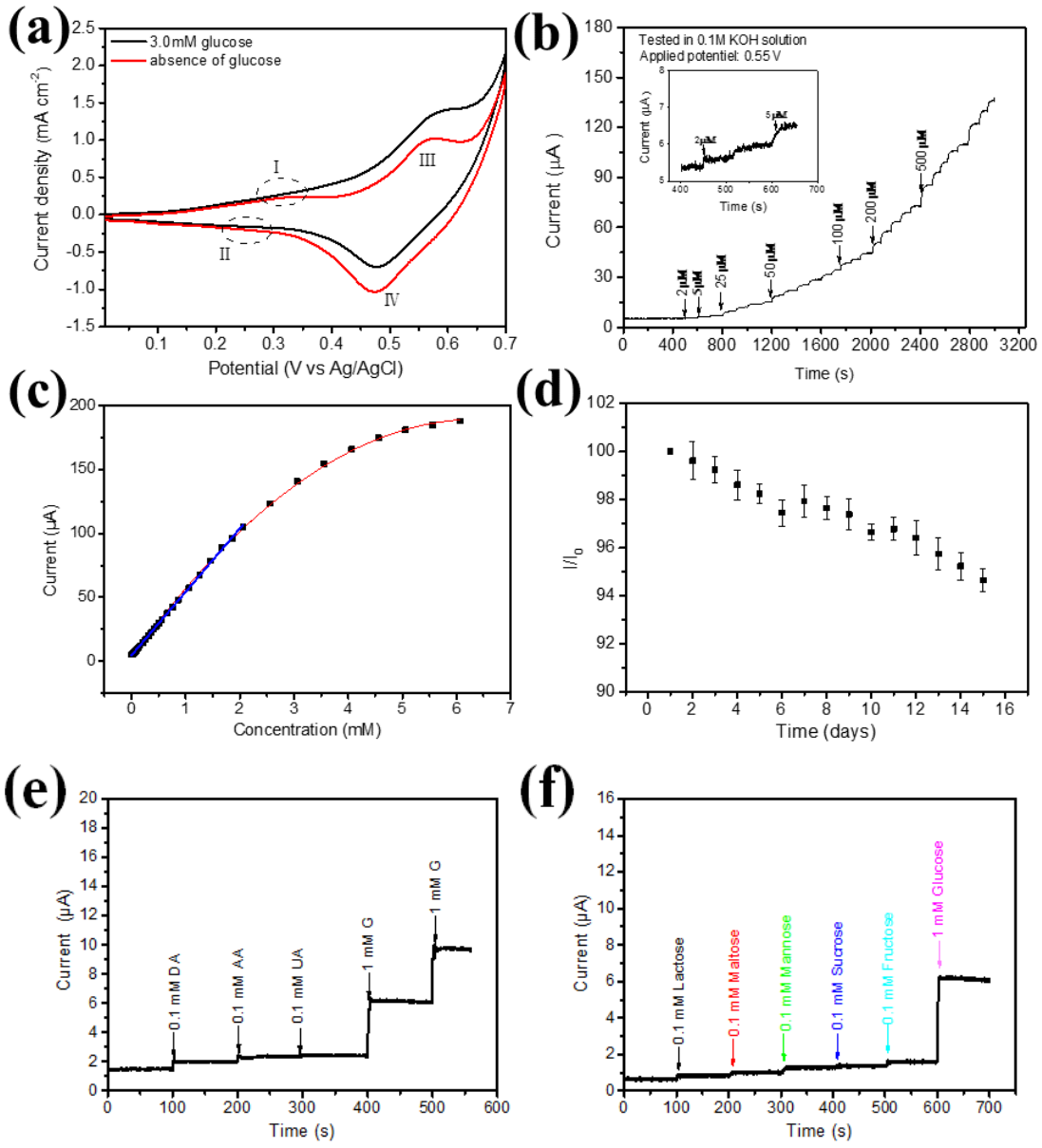

Figure 4. (a) CVs of Co_3O_4-HND/GCE in absence and presence of 3.0 mM glucose; (b) Typical amperometric response of Co_3O_4-HND/GCE at 0.55 V to successive addition of glucose in 0.1 M KOH; (c) The corresponding calibration curve vs. glucose concentration with fitting curve and linear range. (d) Stability of the Co_3O_4-HND electrode stored at ambient conditions in 0.1 M KOH with addition of 0.5 mM glucose at 0.55V; (e) Amperometric response of Co_3O_4-HND/GCE to the successive addition of 0.1 mM DA, 0.1 mM AA, 0.1 mM UA, 1mM glucose; 1mM glucose at the applied potential of 0.55V; (f) Amperometric response of Co_3O_4-HND/GCE to the continuous addition of 0.1 mM Lactose, 0.1 mM Maltose, 0.1 mM Mannose, 0.1 mM Sucrose, 0.1 mM Fructose, and 1mM glucose at a potential of 0.55V.

3.3. Amperometric detection of glucose

It is well known that the applied potential has a strong effect on the sensing performance of the electrochemical sensor. Therefore, the applied potential is critical to achieve the optimal performance for detecting glucose. Constant potential chronoamperomery was carried out by varying the applied potential to investigate the current response with successive addition of 0.1 mM glucose, as demonstrated in Figure S3a. When the applied potential was selected as 0.45, 0.50 V, 0.55 and 0.60 V, one can observe the current response increased accordingly upon each addition of glucose. Given that the background currents and noise signals were more pronounced at 0.6 V, we herein select the potential of 0.55V as the optimum working potential in subsequent tests. The same procedure was performed for the bulk-Co_3O_4 at the suitable potential of 0.55 V. Figure S3b compares the electrochemical response between the Co_3O_4-HND and bulk-Co_3O_4, as a result, the Co_3O_4-HND shows a much higher current response than the bulk-Co_3O_4 upon addition of the same amount of glucose, suggesting the Co_3O_4-HND possess a significantly improved catalytic activity for GOR compared with the bulk Co_3O_4. The real-time amperometric detection of glucose on the Co_3O_4-HND was performed by successive step-wise

addition of different amount of glucose into stirring KOH solution at an applied potential of 0.55V (Figure 4b). Figure 4c shows the corresponding calibration plot relating to the concentration and the current response. The electrochemical oxidation of glucose on Co_3O_4-HND electrode is a surface catalytic reaction(Ding et al. 2010; Lang et al. 2013). Therefore, the equation $I=a\times C_{glucose}/(b+C_{glucose})$ was used to fit the calibration curve based on Langmuir isothermal theory. As depicted in Figure 4c, the calibration data fit this equation very well even over a wide range of 2.0 μM-6.06 mM (R^2=0.999), which can be expressed as the follow equation: $I\ (\mu A)=238.73\times C_{glucose}/(1.81+C_{glucose})$. When glucose concentration is less than 2.1 mM, the equation above can be approximated as $I=49.56\times C_{glucose}$. In this way, the sensitivity is measured to be 708.4 μA mM^{-1} cm^{-2} if only linear range is considered. In addition, the detection limit reached as low as 0.58 μM based on a signal-to-noise ratio of 3 (S/N).

The long-term stability of Co_3O_4-HND/GCE was evaluated by measuring the current responses to 0.5 mM glucose at 0.55 V within half a month period. The electrode was stored in air at room temperature, and its current response was checked every one day. After 15 days of storage, the sensor response current retained about 94.6% of its original value (Figure 4d), indicating the highly operational stability of Co_3O_4-HND electrode. Additionally, the reproducibility and stability of the Co_3O_4-HND electrode for glucose were also investigated. The relative standard deviation (R.S.D.) of 3.9 % (n = 5) for 0.5 mM glucose demonstrated the good intra-electrode reproducibility. On eight Co_3O_4-HND electrodes, the good electrode-to-electrode reproducibility was measured by the low R.S.D. of 5.1 % in the response to 0.5 mM glucose. These results make the Co_3O_4-HND promising for the construction of non-enzymatic glucose sensor.

Selectivity is another major factor to assess the performance of the Co_3O_4-HND electrode for nonenzymatic glucose detection. The selectivity of the Co_3O_4-HND for glucose was evaluated against the normal co-existed interfering species such as dopamine (DA), ascorbic acid (AA), and uric acid (UA). Typically, the physiological

level of glucose is between 4 mM and 7 mM (Park et al. 2006), which is normally 10 times higher than the physiological level of endogenous species like DA, AA and UA (Hrapovic and Luong 2003). Figure 4e showed the amperometric response of the Co_3O_4-HND modified electrode in electrolyte containing 1.0 mM glucose, DA (0.1 mM), AA (0.1 mM) and UA (0.1 mM). At an applied potential of 0.55 V, the electrochemical responses of these electroactive interfering species are almost negligible comparing with that of glucose at the Co_3O_4-HND electrode, suggesting a good selective detection of glucose. Additionally, amperometric response of Co_3O_4-HND electrode to the successive addition of 0.1 mM lactose, 0.1 mM maltose, 0.1 mM mannose, 0.1 mM sucrose, 0.1 mM Fructose, and 1.0 mM glucose as well at a potential of 0.55 V (Figure 4f) , demonstrating the physiological level of saccharides will not affect the detection of glucose. Table S1 listed the enzymeless glucose detection performance with various electrodes related to Cobalt Oxide reported previously, suggesting that Co_3O_4-HND electrode exhibited a higher sensitivity and wider linear range toward glucose oxidation.

3.4. Glucose fuel cell

The excellent catalytic activity of the Co_3O_4-HND toward glucose oxidation offered scientific foundation to design a glucose fuel cell (GFC) device using Co_3O_4-HND as anode material. We herein fabricated an H-type GFC (Figure 5a) using the Co_3O_4-HND as an anode and Pt/C as cathode catalyst, respectively. The output current was altering with time when loading a R_{ex} of 200 Ω in the Co_3O_4-glucose FC. The generated current gradually decreased with the color change of the anode electrolyte, from colorless(similar to cathode solution) to yellow brown (Fig 5a), indicating glucose prevailingly oxidizes to gluconolactone accompanying with 2 electrons transfer per mole of glucose; such catalytic behavior toward glucose oxidation was similar to that of a single enzyme at the anode to oxidize glucose to gluconolactone(Ci et al. 2015a). The Co_3O_4-HND(a||c)-GFC generated a maximum current density of 0.3 mA cm^{-2} in alkaline electrolyte, moreover, a reproducible cycle

of current was obtained upon 2-cycle operation within about 40 hours (Figure 5b), indicating the Co_3O_4-HND was capable of producing steady electricity at milliamps level for a long time.

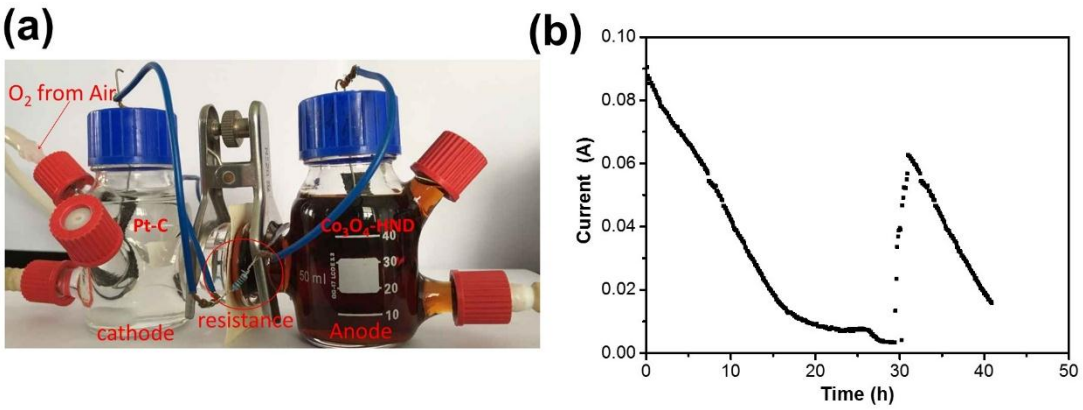

Figure 5. Schematic diagram of the as-designed Co_3O_4-HND(a||c)-GFC (a); Power density curve at room temperature for a nonenzymatic glucose-Air fuel cell, Geometric area: 3 cm^2 (b).

4. Conclusion

In conclusion, the Co_3O_4 with hollow nanododecahedra structure, Co_3O_4-HND, was successfully prepared through heat treatment of the MOF (ZIF-67) precursor in air. The as-obtained Co_3O_4-HND exhibits an outstanding catalytic activity for glucose oxidation. The excellent catalytic activity of the Co_3O_4-HND for GOR inspire us to set up an enzymeless glucose fuel cell, which was capable of producing steady electricity at milliamps level for a long period. The present work not only extend the study in using MOF as template to the fabrication of unique nanostructured metal oxide, but also open a new avenue to exploring MOF-derived energy materials in biofuel cell (BFC).

Acknowledgements: This work was supported by the National Natural Science Foundation of China (21566025 and 21206068) and the Natural Science Foundation of Jiangxi Province (20152ACB21019).

References

Basu, D., Basu, S., 2011. Int J Hydrogen Energ 36, 14923-14929.
Calabrese Barton, S., Gallaway, J., Atanassov, P., 2004. Chem Rev 104, 4867-4886.
Chen, Y., Prasad, K.P., Wang, X., Pang, H., Yan, R., Than, A., Chan-Park, M.B., Chen, P., 2013. Phys Chem Chem Phys 15, 9170-9176.
Ci, S., Huang, T., Wen, Z., Cui, S., Mao, S., Steeber, D.A., Chen, J., 2014. Biosens. Bioelectron. 54, 251-257.
Ci, S., Wen, Z., Mao, S., Hou, Y., Cui, S., He, Z., Chen, J., 2015. Chem. Commun. (Camb) 51, 9354-9357.
Cooney, M., Svoboda, V., Lau, C., Martin, G., Minteer, S., 2008. Energ. Environ. Sci. 1, 320-337.
Ding, Y., Wang, Y., Su, L., Bellagamba, M., Zhang, H., Lei, Y., 2010. Biosens. Bioelectron. 26, 542-548.
Guan, J., Mou, F., Sun, Z., Shi, W., 2010. Chem. Commun. 46, 6605-6607.
Han, L., Yang, D.-P., Liu, A., 2015. Biosens. Bioelectron. 63, 145-152.
Horcajada, P., Chalati, T., Serre, C., Gillet, B., Sebrie, C., Baati, T., Eubank, J.F., Heurtaux, D., Clayette, P., Kreuz, C., 2010. Nat. Mater. 9, 172-178.
Hou, C.C., Li, T.T., Chen, Y., Fu, W.F., 2015. ChemPlusChem.
Hrapovic, S., Luong, J.H., 2003. Anal. Chem. 75, 3308-3315.
Hu, H., Guan, B., Xia, B., Lou, X.W., 2015. J Am Chem Soc 137, 5590-5595.
Huang, G., Zhang, F., Du, X., Qin, Y., Yin, D., Wang, L., 2015. ACS nano 9, 1592-1599.
Kim, S.-W., Kim, M., Lee, W.Y., Hyeon, T., 2002. J Am Chem Soc 124, 7642-7643.
Lang, X.-Y., Fu, H.-Y., Hou, C., Han, G.-F., Yang, P., Liu, Y.-B., Jiang, Q., 2013. Nature commun. 4.
Lee, J., Farha, O.K., Roberts, J., Scheidt, K.A., Nguyen, S.T., Hupp, J.T., 2009. Chem. Soc. Rev. 38, 1450-1459.
Li, J.-R., Sculley, J., Zhou, H.-C., 2011a. Chem. Rev. 112, 869-932.
Li, M., Han, C., Zhang, Y., Bo, X., Guo, L., 2015. Analytica Chimica Acta 861, 25-35.
Li, Q., Guo, B., Yu, J., Ran, J., Zhang, B., Yan, H., Gong, J.R., 2011b. J Am Chem Soc 133, 10878-10884.
Li, Y.Y., Cunin, F., Link, J.R., Gao, T., Betts, R.E., Reiver, S.H., Chin, V., Bhatia, S.N., Sailor, M.J., 2003. Science 299, 2045-2047.
Lou, X.W., Wang, Y., Yuan, C., Lee, J.Y., Archer, L.A., 2006. Adv. Mater. 18, 2325-2329.
Lü, Y., Zhan, W., He, Y., Wang, Y., Kong, X., Kuang, Q., Xie, Z., Zheng, L., 2014. Acs. Appl. Mater.Inter. 6, 4186-4195.
Madhu, R., Veeramani, V., Chen, S.-M., Manikandan, A., Lo, A.-Y., Chueh, Y.-L., 2015. Acs. Appl. Mater.Inter.

Mu, Y., Jia, D., He, Y., Miao, Y., Wu, H.-L., 2011. Biosens. Bioelectron. 26, 2948-2952.
Park, S., Boo, H., Chung, T.D., 2006. Analytica Chimica Acta 556, 46-57.
Sculley, J., Yuan, D., Zhou, H.-C., 2011. Energ. Environ. Sci. 4, 2721-2735.
Shao, J., Wan, Z., Liu, H., Zheng, H., Gao, T., Shen, M., Qu, Q., Zheng, H., 2014. J. Mater. Chem. A 2, 12194-12200.
Si, P., Huang, Y., Wang, T., Ma, J., 2013. Rsc Advances 3, 3487-3502.
Song, J., Xu, L., Zhou, C., Xing, R., Dai, Q., Liu, D., Song, H., 2013. Acs. Appl. Mater.Inter. 5, 12928-12934.
Wang, B., Lu, X.-Y., Tang, Y., 2015. Journal of Materials Chemistry A 3, 9689-9699.
Wang, G., He, X., Wang, L., Gu, A., Huang, Y., Fang, B., Geng, B., Zhang, X., 2013. Microchimica Acta 180, 161-186.
Wang, X., Dong, X., Wen, Y., Li, C., Xiong, Q., Chen, P., 2012. Chem. Commun. 48, 6490-6492.
Wu, R., Qian, X., Rui, X., Liu, H., Yadian, B., Zhou, K., Wei, J., Yan, Q., Feng, X.Q., Long, Y., 2014. Small 10, 1932-1938.
Yang, P., Tong, X., Wang, G., Gao, Z., Guo, X., Qin, Y., 2015. Acs. Appl. Mater.Inter 7, 4772-4777.
Yuhashi, N., Tomiyama, M., Okuda, J., Igarashi, S., Ikebukuro, K., Sode, K., 2005. Biosens. Bioelectron. 20, 2145-2150.
Zhang, C., Qian, L., Zhang, K., Yuan, S., Xiao, J., Wang, S., 2015. J. Mater. Chem.A 3, 10519-10525.
Zhang, Y.-Z., Wang, Y., Xie, Y.-L., Cheng, T., Lai, W.-Y., Pang, H., Huang, W., 2014. Nanoscale 6, 14354-14359.

Highlights (BIOS-D-15-02965)

(1) Developing a reliable strategy to fabricate a hollow structured cobalt oxide nanododecahedras (Co_3O_4-HND), which shows fascinating physical and chemical features;

(2) The Co_3O_4-HND shows significantly improved activity toward catalyzing glucose oxidation reaction compared with the bulk Co_3O_4;

(3) A high-performance glucose biosensor and biofuel cell was set up with the Co_3O_4-HND as the electrode material.